Journal of Translational Medicine

RESEARCH

Open Access

# Single-cell transcriptomic analysis reveals characteristic feature of macrophage reprogramming in liver Mallory-Denk bodies pathogenesis

Zixuan Fang[1,2†], Bei Zhong[1†], Yi Shi[1,2], Wanmei Zhou[1,2], Maoping Huang[1], Samuel W. French[3], Xiaoping Tang[2,4*] and Hui Liu[1,2,5*]

## Abstract

Chronic liver diseases are highly linked with mitochondrial dysfunction and macrophage infiltration. Mallory-Denk bodies (MDBs) are protein aggregates associated with hepatic inflammation, and MDBs pathogenesis could be induced in mice by feeding 3,5-diethoxycarbonyl-1,4-dihydrocollidine (DDC). Here, we investigate the macrophage heterogeneity and the role of macrophage during MDBs pathogenesis on DDC-induced MDBs mouse model by single-nucleus RNA sequencing (snRNA-seq). We defined liver macrophages into four distinct subsets including monocyte-derived macrophages (MDMs) subset and three Kupffer cells (KCs) subsets (Gpnmb$^{high}$ KCs, Peam1$^{high}$ KCs, and Gpnmb$^{low}$ Pecam1$^{low}$ KCs). Particularly, we identified a novel Gpnmb$^{high}$ KCs subset as lipid-associated macrophage (LAM) with high expression of Trem2, CD63, and CD9. Interestingly, LAM showed a potential immunosuppressive characteristic by expressing anti-inflammatory genes IL-7R during the MDBs formation. Using contact and transwell co-culture systems, the released mtDNA from hepatocytes was found to induce the activation of inflammasome in macrophages. Furthermore, we revealed the damaged DNA could activate the NOD-like receptor family pyrin domain containing-3 (NLRP3) inflammasome and subsequently form apoptosis-associated speck-like protein containing a caspase recruit domain (ASC) specks of liver macrophages. Collectively, our results firstly revealed macrophage heterogeneity and inflammasome activation by mtDNA from injured liver during MDBs pathogenesis, providing crucial understanding of pathogenesis of chronic liver disease.

**Keywords** Mallory-denk bodies (MDBs), Lipid-associated macrophage, Single-nucleus RNA-sequencing, mtDNA, Inflammasome

†Zixuan Fang and Bei Zhong contributed equally to this work.

*Correspondence:
Xiaoping Tang
tangxp@gzhmu.edu.cn
Hui Liu
liuhui806@gzhmu.edu.cn
[1]The Fifth Affiliated Hospital of Guangzhou Medical University, Guangzhou, China; The Qingyuan Affiliated Hospital of Guangzhou Medical University, Qingyuan People's hospital, Qingyuan, China
[2]The State Key Laboratory of Respiratory Disease and National Clinical Research Center for Respiratory Disease, Guangzhou, China
[3]Department of Pathology, Harbor UCLA Medical Center, University of California, Torrance CA90502, USA
[4]Research Institute of Infectious Diseases, Guangzhou Eighth People's Hospital, Guangzhou Medical University, Guangzhou, China
[5]Guangdong Provincial Key Laboratory of Allergy & Clinical Immunology, The Second Affiliated Hospital of Guangzhou Medical University, Guangzhou, China

## Introduction

Mallory-Denk bodies (MDBs) are protein aggregates described as the morphological feature of alcoholic steatohepatitis (ASH) and non-alcoholic steatohepatitis (NASH), the pathogenesis of which has also been linked to cellular stress and aging [1–3]. Similarly, the formation of MDBs-like cytoplasmic inclusions also occurred in neurodegenerative diseases such as Alzheimer's, Parkinson's and Desmin-related myopathies [4]. MDBs are the inclusions commonly seen in hepatocellular carcinoma (HCC), therefore the acknowledgment of MDBs pathogenesis helps to better understand the HCC progression and neurodegenerative diseases [5, 6]. MDBs formation can be induced in mice by chronic dietary administration of 3,5-diethoxycarbonyl-1,4-dihydrocollidine (DDC) and griseofulvin [7, 8]. The DDC mouse model has become the gold standard for elucidating the pathogenesis of MDBs [8]. The main components of MDBs include p62, keratins 8/18 (Krt8/18), and ubiquitin [9]. The relevant pathogenesis leading to MDBs formation includes protein misfolding and consequent proteasome overload, epigenetic mechanisms, and chronic activation of proinflammatory pathways such as NF-κB and Toll-like signaling pathways [9, 10]. However, the molecular mechanisms of MDBs formation are not fully understood.

Macrophages, as the most numerous immune cells in the liver, depending on their high plasticity play a crucial role in inflammation. During chronic liver disease, macrophages express proinflammatory cytokines such as TNFα and IL-1β to induce cell injury [11, 12]. Cytokines IFNγ could enhance the TNFα/TNFR1 signaling pathway resulting in the FAT10 expression in macrophages [13], while in vitro study showed that the FAT10 positive hepatocytes could form MDBs-like aggresomes [14]. Interestingly, it was found that the liver cells with MDBs formation were surrounded by numerous CD163-positive M2a macrophages in patients with alcoholic hepatitis (AH) [15]. Moreover, a study of non-alcoholic fatty liver disease (NAFLD) pathogenesis showed that M1 phenotype macrophages were highly involved in p62-positive inclusions [16]. This implies macrophages have a close relationship with the MDBs pathogenesis. As liver disease develops, macrophages become activated in response to environmental stimuli by sensing pathogen-associated molecular patterns (PAMPs) and danger-associated molecular patterns (DAMPs) released by damaged cells, leading to infiltration and macrophage polarization [17–19]. Mitochondrial DNA (mtDNA) is a double-stranded circular loop DNA and participates in the synthesis of respiratory chain complexes [20], and it could act as DAMPs to leave mitochondria during mitochondrial dysfunction and then trigger inflammation [21–23]. A clinical study has shown that MDBs formation can result in the severity of inflammasome activation in AH [24]. Nevertheless, the molecular process of the macrophage activation associated with mtDNA release following chronic liver injury during MDBs formation remains unclear.

High-throughput sequencing technology emerged as a powerful tool for revealing cell heterogeneity and has enabled the description of immune cells on single cell level. Compared to single-cell RNA sequencing (scRNA-Seq), single-nucleus RNA sequencing (snRNA-seq) gets a more comprehensive proportion of all cell types and works better for liver parenchymal cells [25–27]. In addition, our recent studies have illustrated a comprehensive understanding of liver macrophages in C57BL/6 mice following DDC chronic injury [28]. In this study, we performed snRNA-seq on the DDC-induced MDBs mouse model to characterize the reprogramming of macrophage heterogeneity during MDBs formation. We defined a novel lipid-associated macrophage (LAM) subset of high expression of Gpnmb and Trem2 with anti-inflammation characteristics. Interestingly, IL-7R was found to be significantly upregulated in this LAM subpopulation. Furthermore, we found inflammasome activation induced by damaged DNA in mice and verified macrophage NOD-like receptor family pyrin domain containing-3 (NLRP3) activation by mtDNA release from hepatocytes in vitro. Taken together, our results illustrated the significant heterogeneity of macrophages and inflammasome activation resulted from injured liver during MDBs pathogenesis, providing a novel insight into the understanding of chronic liver disease.

## Materials and methods

### Animal experiments

All male mice were on a C3H background and purchased from Beijing Vital River Laboratory Animal Technology. All mice were bred in a specific-pathogen-free (SPF) environment with free access to food and water and housed in standard conditions of 20–26 °C temperature and 40–70% humidity under a 12 h light cycle at Guangzhou Medical University. All animal experiments protocols used in this study were approved by the Animal Care Committee of the Guangzhou Medical University (GY2022144). Consistent with previous research [7], the Control mice ($n = 3$) were fed with a complete standard Control diet. For MDBs model mice, the DDC-Fed mice ($n = 3$) were fed the Control diet and added 0.1% DDC (Sigma-Aldrich, 137030-25G) for 10 weeks to induce the formation of MDBs. They were then withdrawn from DDC for 1 month ($n = 3$), at which time the MDBs had mostly disappeared. They were then refed DDC ($n = 3$) for 6 to 10 days as was previously done [7]. Then the liver tissue from each group was obtained for subsequent experiments: (1) liver tissue was subjected to nuclei isolation and snRNA-seq; (2) Tissue was cut into distinct small

sections and preserved in 4% polyformaldehyde for subsequent immunostaining; (3) liver tissue and serum were preserved at -80 °C for RNA and protein lysates extracting, ELISA, qPCR and Western blot analysis.

#### Patients and clinical specimens

Human formalin-fixed paraffin-embedded (FFPE) liver biopsies from patients with HCC ($n = 3$) were obtained from the Qingyuan Affiliated Hospital of Guangzhou Medical University archives, with Institutional Review Board approval (IRB-2022-094). The patients exhibited features of MDBs on liver histopathology and the details were shown in Table 1. The liver biopsy sections were 4 μm thick. The study was carried out according to the principles of the Declaration of Helsinki and the data were analyzed anonymously and reported.

#### Single-nucleus RNA-Sequencing (snRNA-seq) and bioinformatics

Nuclei isolation and snRNA-seq dataset of 10× Genomics® as standard protocol as described previously [28] and data analysis was mainly performed by Genedenovo Biotechnology Co., Ltd (Guangzhou, China). Clustering analysis composed of R package Seurat was used to perform quality control and exploration of snRNA-seq data. Then, Seurat continued to use Uniform manifold approximation and projection (UMAP) to visualize and explore these datasets. The differentially expressed gene analysis and expression value of each gene in the given cluster were compared against the rest of cells using the Wilcoxon rank sum test. Kyoto Encyclopedia of Genes and Genomes (KEGG) was used to further understand the biological functions of genes and pathway enrichment analysis. Gene set variation analysis (GSVA) was performed by the "GSVA" R package for GSVA enrichment analysis.

#### Hematoxylin and eosin (H&E) staining

H&E staining was performed following a standard protocol for mice liver tissue sections. Briefly, liver sections were deparaffinized with TO and then hydrated in decreasing concentrations of alcohol for subsequent staining. The liver sections were stained in hematoxylin solution for 3 min and then washed in PBS of 0.1% Tween-20 for 5 min. Next, the slides were put into eosin solution for 2 min to stain the cytoplasm. After washing for 5 min in tap water, the sections were dehydrated and then a drop of mounting medium was added to mount each of the liver tissue. Images were collected by slide scanner systems PRECICE 500 (UNIC) and processed by iViewer software (UNIC).

**Table 1** Liver and serum parameters in 3 HCC samples which had formed MDBs

| | HCC#1 | HCC#2 | HCC#3 |
|---|---|---|---|
| Gender | Female | Male | Male |
| Age | 44 | 62 | 48 |
| ALT(U/L) | 20 | 37 | 11 |
| AST(U/L) | 29 | 29 | 20 |
| ALP(U/L) | 74 | 80 | 108 |
| AFP(U/L) | > 1210 | > 1210 | 905 |
| CK8/18 | + | + | + |
| MDBs | +++ | +++ | +++ |

#### Immunohistochemical assay

Liver sections were deparaffinized with TO and hydrated in decreasing concentrations of alcohol. Antigen epitope retrieval was performed by microwave heating within a citrate antigen retrieval solution (Beyotime, P0081). The sections were incubated with 0.3%$H_2O_2$ for 15 min and blocked in PBS of 5%BSA for 1 h at room temperature (RT). Next, sections were stained with mouse anti-F4/80 (Bioss, bsm-34028 M) or rabbit anti-IL-7R (Bioss, bs-1540R) overnight at 4 °C. After washing, sections were incubated with HRP-conjugated secondary antibodies for 1 h. Then, the signal was detected using a DAB kit (ZSGB-Bio, ZLI-9018). At last, the sections were counterstained with hematoxylin. Images were collected by slide scanner systems PRECICE 500 (UNIC) and then processed by iViewer software (UNIC).

#### RNA extraction and quantitative PCR (qPCR)

Total cells and tissue RNA were extracted as indicated using Cell/Tissue Total RNA Kit (Yeason, 19221ES50) and then reverse-transcribed into cDNA using 5×HiScript III qRT SuperMix (Vazyme, R323-01). qPCR was performed using TB Green® Premix Ex Taq™ II (TaKaRa, RR820A) with the primers listed in Table 2.

#### Immunofluorescence

After deparaffinization and antigen retrieval in darkness, liver sections were blocked in PBS of 5% BSA for 1 h at RT. Autofluorescence was quenched using a tissue autofluo quencher (Servicebio, G1221), followed by washing PBS of 0.1% Tween-20 three times (3 min/per). Sections were incubated with rabbit anti-F4/80; rabbit anti-IL-7R, rabbit anti-GPNMB (Bioss, bs-2684R); rabbit anti-8-OHdG (Bioss, bs-1278R); rabbit anti-ASC (CST, #67824); rabbit anti-KRT8 (Abcam, ab55407 (Red); or proteintech, 27105-1-AP (Green)), mouse anti-nucleoporin p62 (Santacruz, sc-48373) at 4 °C overnight. Sections were washed and incubated with Alexa Fluor 488 goat anti-rabbit IgG (Invitrogen, A11008), Alexa Fluor 488 goat anti-mouse IgG (Invitrogen, A11001), Alexa Fluor 555 goat anti-rabbit IgG (Invitrogen, A21428), Alexa Fluor 555 goat anti-mouse IgG (Invitrogen, A21422) and Alexa Fluor 647 donkey anti-rabbit IgG (Invitrogen, A31573)

**Table 2** Sets of specific oligonucleotide quantitative real-time PCR (qRT-PCR) primers

| Gene | Species | Forward sequence(5'to3') | Reverse sequence(5'to3') |
|---|---|---|---|
| Gapdh | Mouse | AGGTCGGTGTGAACGGATTTG | TGTAGACCATGTAGTTGAGGTCA |
| FAT10 (UbD) | Mouse | GATTGACAAGGAAACCACTATCCA | ACAAGGGCAGCTCTTCATCAC |
| Krt8 | Mouse | TCCATCAGGGTGACTCAGAAA | CCAGCTTCAAGGGGCTCAA |
| p62 (Sqstm1) | Mouse | AAGTCAGCAAACCTGACG | CCATCTGTTCCTCTGGCT |
| CD86 | Mouse | TGTTTCCGTGGAGACGCAAG | TTGAGCCTTTGTAAATGGGCA |
| NOS2 | Mouse | CAAGCTGAACTTGAGCGAGGA | TTTACTCAGTGCCAGAAGCTGGA |
| TNFα | Mouse | CCCTCACACTCAGATCATCTTCT | GCTACGACGTGGGCTACAG |
| IFNγ | Mouse | ATGAACGCTACACACTGCATC | CCATCCTTTTGCCAGTTCCTC |
| Argl | Mouse | AGCTCTGGGAATCTGCATGG | ATGTACACGATGTCTTTGGCAGATA |
| Mrc1 | Mouse | AGCTTCATCTTCGGGCCTTTG | GGTGACCACTCCTGCTGCTTTAG |
| IL-7R | Mouse | GCGGACGATCACTCCTTCTG | AGCCCCACATATTTGAAATTCCA |
| Trem2 | Mouse | CTGGAACCGTCACCATCACTC | CGAAACTCGATGACTCCTCGG |
| Gpnmb | Mouse | GCTGGTCTTCGGATGAAAATGA | CCACAAAGGTGATATTGGAACCC |
| CD9 | Mouse | ATGCCGGTCAAAGGAGGTAG | GCCATAGTCCAATAGCAAGCA |
| CD63 | Mouse | GAAGCAGGCCATTACCCATGA | TGACTTCACCTGGTCTCTAAACA |
| CD200 | Mouse | CTCTCCACCTACAGCCTGATT | AGAACATCGTAAGGATGCAGTTG |
| Pacrg | Mouse | CTGCCACAACAGACGTTCCA | ATTTTCGGAAAGTGGTGGGTT |
| Anxa1 | Mouse | ATGTATCCTCGGATGTTGCTGC | TGAGCATTGGTCCTCTTGGTA |
| Nlrp3 | Mouse | ATTACCCGCCCGAGAAAGG | TCGCAGCAAAGATCCACACAG |
| Pycard | Mouse | CTTGTCAGGGGGATGAACTCAAAA | GCCATACGACTCCAGATAGTAGC |
| Casp-1 | Mouse | ACAAGGCACGGGACCTATG | TCCCAGTCAGTCCTGGAAATG |
| IL-1β | Mouse | GCAACTGTTCCTGAACTCAACT | ATCTTTTGGGGTCCGTCAACT |
| IL-18 | Mouse | GACTCTTGCGTCAACTTCAAGG | CAGGCTGTCTTTTGTCAACGA |

for 1 h. The sections were then stained with DAPI (Beyotime, c1002) for 5 min and washed in PBS of 0.1%Tween-20 for 5 min three times before mounting with Antifade Mounting Medium (Beyotime, P0128M). Images were observed and snapped by laser confocal microscope (ZEISS, LSM880) equipped with photomultiplier tube (PMT) detectors. The pictures were then processed by ZEN software (ZEISS) at a resolution of 1024 × 1024 pixels.

#### Transmission electron microscopical analysis

For transmission electron microscopy, the liver tissue from the Control and DDC-Fed mice were sliced into 1 $mm^3$ sections fixed with 2.5% glutaraldehyde (PH7.4) for 2 h. After washing with 0.1 M phosphate buffer (pH 7.2) for 3 times, the tissue were then fixed in 1% osmic acid for 2 h at 4℃. Next, the sections were hydrated in decreasing concentrations of alcohol and subsequently embedded in Epon-Araldite resin (Ted Pella Inc). The ultrathin sections were cut using a Leica EM UC7 Ultramicrotome (Leica, LeicaUC7) and then counterstained with 3% uranyl acetate and 2.7% lead citrate. The sections were observed using a JEM1400 transmission electron microscope (JEOL, JEM1400) and operated at 80 kV.

#### MDBs induction in vitro

This experiment was repeated and improved the long-term treatment of hepa1-6 described previously [14]. $8 \times 10^6$ cells were seeded in 12-well Cell Culture Plates or 10-cm cell culture dishes. The hepa1-6 cells were continuously co-stimulated with 40ng/ml TNFα (PeproTech, 315–01 A) and 400ng/ml IFNγ (novoprotein, C746) for 10 days with intervals of three days. The cytokine and medium were refreshed every three days, then the cells were harvested for immunofluorescence and qPCR at day 10.

#### Raw264.7/Hepa1-6 contact co-culture and mitochondrial labelling

Raw264.7 cells were cultured in Dulbecco's modified Eagle's medium (DMEM, Gibco, 11965092) containing 1% penicillin/streptomycin and 10% FBS (Excell, FSS500). Hepa1-6 were cultured in DMEM ($NAHCO_3$ concentration of 1.5/L, iCell-128-000) supplemented with 5% FBS. All cells were cultured under a humidified atmosphere with 5% $CO_2$ at 37 °C. Raw264.7 cells were seeded in 12-well chambered cell culture slides (CITOTEST) for 12 h before initiation of the co-culture. Hepa1-6 cells and MDB-forming hepa1-6 cells were seeded in 6-well plates at a density of 150,000 cells per well in a 1:1 ratio and stained for 30 min using Mitotracker (Invitrogen, M7512) after culturing overnight for draining the excess dye. Then the stained hepa1-6 cells were added to the preseeded Raw264.7 cells and contact co-cultures were maintained for 24 h in DMEM with 1.5 g/L $NAHCO_3$.

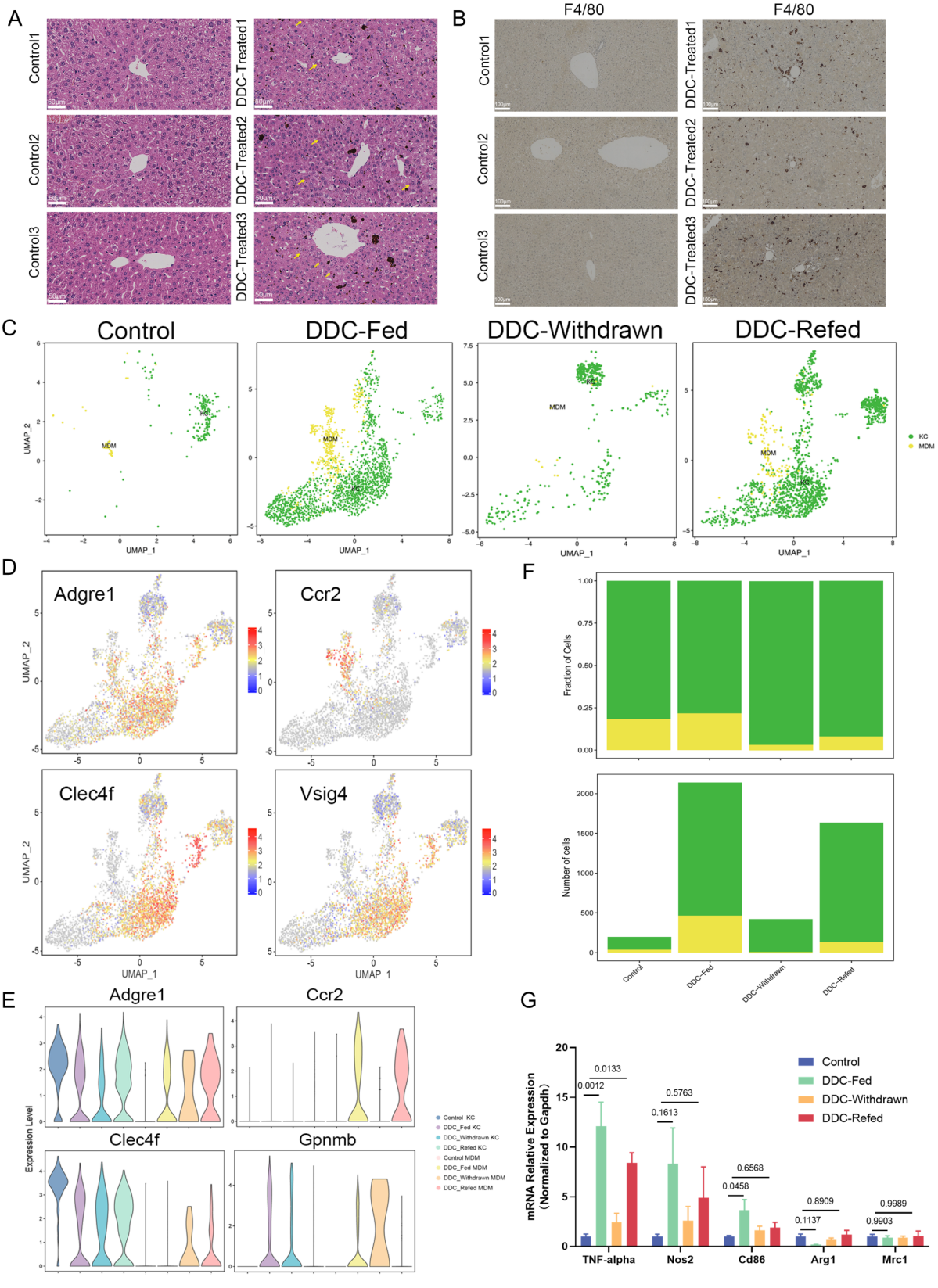


**Fig. 1** (See legend on next page.)

(See figure on previous page.)

**Fig. 1** The phenotype changes in the MDBs pathogenesis. (**A**) Liver tissue sections of Control and DDC-Fed mice were stained with hematoxylin-eosin (H&E). The yellow arrow indicates the MDBs. Scale bar, 50 μm. (**B**) Immunohistochemical analysis of F4/80 expression in liver tissue sections is shown. Scale bar, 50 μm. (**C**) UMAP visualization illustrates cell types of KCs (green) and MDM (yellow) among Control, DDC-Fed, DDC-Withdrawn, and DDC-Refed mouse livers. (**D**) UMAP plot illustrating feature plots of subtype-specific genes expression. (**E**) Violin plot showing the distribution of marker genes Adgre1, Ccr2, Clec4f, and Gpnmb expression. (**F**) Total cell counts and percentage contributions from Control, DDC-Fed, DDC-Withdrawn, and DDC-Refed mouse livers for each subcluster are shown. (**G**) M1 phenotype genes and M2 phenotype genes were detected in Control, DDC-Fed, DDC-Withdrawn, and DDC-Refed mice liver tissue by qPCR. The data presented are representative of three independent experiments. The DDC-Fed and DDC-Refed groups were compared to the Control group. Data are shown as mean ± SEM, and P-values were determined by one-way ANOVA of independent biological experiments ($n = 3$)

#### Western blot

Proteins extracted from the liver tissues by RIPA lysis buffer (Beyotime, P0013B) with protease cocktail inhibitor I (Apexbio, K1007). Lysates were mixed with 5× SDS Loading buffer and boiled at 100 °C for 10 min. Then, they were separated on SDS-PAGE (10%polyacrylamide) and transferred to polyvinylidene fluoride membranes (PVDF) (Millipore, ISEQ00010). The proteins solution were mixed with anti-NLRP3 rabbit mAb (Abcam, EPR23094-1), ASC rabbit mAb, Pro-Caspase-1 rabbit mAb (MCE, HY-P80587), Cleaved-Caspase-1 rabbit mAb (MCE, HY-P80622), IL-1β rabbit mAb (Abclonal, A16288), β-actin mouse mAb (Proteintech, HRP-66009), α-tubulin (Beyotime, AT-819-1) and GAPDH mouse mAb (Proteintech, 60004-1-Ig). HRP-conjugated secondary antibodies were used for protein detection, followed by exposure to the chemiluminescence imaging system Pxi9 (Syngene) and then images were processed with ImageJ software.

#### Enzyme-linked immunosorbent assay (ELISA)

This analysis was performed following a standard protocol provided by ELISA kit (Thermo, 88–7013 A-88). The optical density (OD) of all samples to be tested (liver protein lysates and cell culture supernatant) was determined by VARIOSKAN FlASH (Thermo) at 450 nm. The data were processed by GraphPad Prism version 9.0 (GraphPad Software, California, USA).

#### Raw264.7/Hepa1-6 Transwell coculture system

Total $1 \times 10^6$ Control hepa1-6 or MDBs hepa1-6 cell model described above was added to the upper chamber of Transwell-24 inserts (6.5 mm diameter with polycarbonate membrane filters containing 3 μm pores, Nest, CN) and allowed them to attach for 12 h at 37 °C and 5% $CO_2$. The medium was removed and replaced with 100 μL of DMEM ($NaHCO_3$ concentration of 1.5/L with 5% FBS) to support cell survival, and then the transwell inserts containing hepa1-6 cells were transferred to Raw264.7 macrophage-seeded wells ($n = 3$ per phenotype). LPS-primed Raw264.7 cells were stimulated by 100ng/ml LPS (Sigma, L2630) for 24 h to initiate macrophage activation. The lower compartment contained high glucose DMEM supplemented with 10% FBS. The cells and supernatants were harvested after coculturing for 24 h and were lysed with 350 μl LB Buffer (Yeasen, CN) and subjected to qPCR and ELISA analysis.

#### Statistical analysis

The data of all quantitative in vitro and in vivo experiments (three mice per group) are represented as mean ± SEM or SD of three independent experiments. $P$-value < 0.05 was considered statistically significant. All statistical analyses using the GraphPad Prism version 9.0 (GraphPad Software, California, USA).

#### Data Availability

SnRNA-seq data generated in this work have been deposited in the GEO with assigned accession numbers GSE201569. These data will be also available from the corresponding author upon request.

## Results

#### MDBs formation induced the reprogramming of macrophages

A well-established MDBs mouse model as we previously done [7, 28] was used to illustrate the mechanisms during MDBs pathogenesis from liver tissue of Control and DDC-treated groups. H&E staining of the DDC-Fed livers showed that the protein of aggregated MDBs was mostly located near the nucleus, and more inflammation and hepatocellular ballooning could be observed (Fig. 1A). The significant F4/80 staining signals were exhibited in the DDC-Fed mice livers compared to Control by immunohistochemistry (IHC) analysis (Fig. 1B), implying the higher-grade inflammatory infiltration of macrophages during this process. We then employed snRNA-seq analysis on the livers of each group and analyzed macrophage heterogeneity. After stringent filtering, this macrophage cluster (4427 cells) could be further grouped by two distinct kupffer cells (KCs) and monocyte-derived macrophages (MDMs) macrophage subsets (Fig. 1C) according to their marker gene expression profile (Fig. 1D). KCs were characterized by Clec4f and Vsig4, and MDMs expressed high levels of Ccr2 and Cx3cr1 [29, 30]. The violin plot showed the high expression of marker gene expression in KC and MDM of four groups. Interestingly, an endogenous glycoprotein encoding gene, Gpnmb, was highly upregulated in KCs (Fig. 1E). Remarkably, a distinctive feature

is the expansion of the macrophage population present in the DDC-Fed liver. Among these, KCs accounted for the majority of the macrophage populations 78% and 91.96% in DDC-Fed and DDC-Refed liver tissue respectively (Fig. 1F; Table 3). qPCR was performed on mice and showed the pro-inflammatory related factors such as CD86, NOS2, and TNFα were upregulated in the liver compared to the Control group (Fig. 1G). However, the expression of Arg1 and Mrc1 (encoding CD206) in M2 phenotype were downregulated. Consistent with the liver immune microenvironment during AH and NASH [31, 32], our data suggested the expansion of macrophages and the highly heterogeneous changes during the MDBs formation.

#### Identification and characterization of macrophage subsets

We next performed clustering analysis and further identified KCs into three groups including Gpnmb$^{high}$ KC, Pecam1$^{high}$ KC, and Gpnmb$^{low}$ Pecam1$^{low}$ KC (Fig. 2A). The feature genes were shown by UMAP (Fig. 2B). The number of each macrophage group exhibited a prominent expansion upon DDC treatment (Fig. 2C, left; Table 4). Remarkably, we revealed a distinct Gpnmb$^{high}$ population constituting 24% of macrophages in the DDC-Fed liver, and almost a complete absence in the Control liver (Fig. 2C, right), implying that the subset was highly associated with MDBs formation. KEGG analysis of this Gpnmb$^{high}$ subset revealed the signatures were associated with the phagosome, lysosome, mTOR signaling pathway and cholesterol metabolism (Fig. 2D). Gene set variation analysis (GSVA) showed that this subset was mainly involved in cholesterol homeostasis and inflammatory pathways including IL2-STAT5 signaling pathways (Fig. 2E). Increased lipid synthesis was associated with enhanced phagocytosis mediated by activation of the mTOR pathway and the transcriptome is similar to the subcluster described previously [33, 34]. Therefore, we termed this novel subset "Lipid-associated Macrophage" (LAM). Subcluster MDM top 10 DEGs showed the enrichment of major histocompatibility complex II (MHC II) genes such as Cd74, Ccr2, H2-Ab1, and H2-Eb1 (Fig. 2F). Furthermore, the KEGG terms enriched for this MDM subcluster was associated with ribosome, osteoclast differentiation, Th1 and Th2 cell differentiation, Th17 cell differentiation, and antigen processing and presentation (Fig. 2G). GSVA in the MDM subset also revealed the activation of TNFα signaling via NF-κB, IFNγ response, IL6/STAT3 (Fig. 2E), and the NF-κB activation has already been verified to promote MDBs aggresome [10]. It indicated that MDM subset may be highly linked with inflammatory pathways contributing to the MDBs pathogenesis. PECAM1 is commonly expressed in immune cells including monocytes, neutrophils, T cells, B cells, macrophages, and endothelial cells [35]. Notably, we recognized Pecam1$^{high}$ KC subcluster which was mainly derived from endothelial cells, and the KEGG terms enriched for this subtype were related to focal adhesion, adherens junction, and Rap1 signaling pathway (Fig. 2H). GSVA indicated that the Pecam1$^{high}$ KC signature was closely associated with WNT, TGF, and P53 pathways (Fig. 2E), so we considered that this subcluster may regulate cell movement, proliferation, and macrophage infiltration. Moreover, we found that the Gpnmb$^{low}$ Pecam1$^{low}$ KC expressed a high level of Timd4 and complement genes (C6 and C4b) (Fig. 2F). The KEGG terms enriched in Gpnmb$^{low}$ Pecam1$^{low}$ KC were related to complement and coagulation cascades, PPAR signaling pathway, metabolic pathways, cholesterol metabolism, platelet activation (Fig. 2I). GSVA was further displayed in this subcluster mainly involved in xenobiotic, fatty, bile acid and glycogen metabolism(Fig. 2E), so we accordingly considered that this subcluster engaged immune regulation and metabolism in inflammation. Taken together, these results illustrate profound functional reprogramming in macrophages during MDBs pathogenies.

**Table 3** The proportional change of KCs and MDMs subsets in the control, DDC-Fed, DDC-Withdrawn and DDC-Refed samples

| Cluster | Control | DDC-Fed | DDC-Withdrawn | DDC-Refed |
|---|---|---|---|---|
| Total | 197 (100%) | 2140 (100%) | 435 (100%) | 1655 (100%) |
| KC | 161 (81.73%) | 1676(78.32%) | 421(96.78%) | 1522(91.96%) |
| MDM | 36 (18.27%) | 464 (21.68%) | 14 (3.22%) | 133 (8.04%) |

#### Immunosuppressive genes were enriched in LAM during MDBs formation

To better understand the role of LAM during MDBs pathogenesis, we next examined surface markers of the classic LAM population and UMAP showed that this subcluster was enriched by the expression of Trem2, Cd63, and Cd9 (Fig. 3A). Notably, this LAM subset in our dataset showed a similar signature with the Trem2$^+$ Cd63$^+$ Cd9$^+$ Gpnmb$^+$ classic lipid-associated macrophages identified in recent studies of mouse and human livers [36]. These special macrophages could be recruited to the steatotic regions of the liver in steatosis [34], while apoptotic steatotic hepatocytes could promote the phagocytosis of macrophages [37]. MDBs were mostly observed in ballooning hepatocytes, and we therefore considered a high association between LAM and MDBs pathogenesis. We next analyzed the transcriptional signature of LAM and found that it was characterized by IL-7R, Cd200, and Anxa1 according to their top 10 DEG. Interestingly, these genes were defined with anti-inflammatory features [38–40]. Then, we used UMAP to validate the expression of M2 phenotype marker Mrc1 (Cd206), while gene expression of M1 phenotype disappeared in this LAM subcluster (Fig. 3B). It suggested a possible switch to

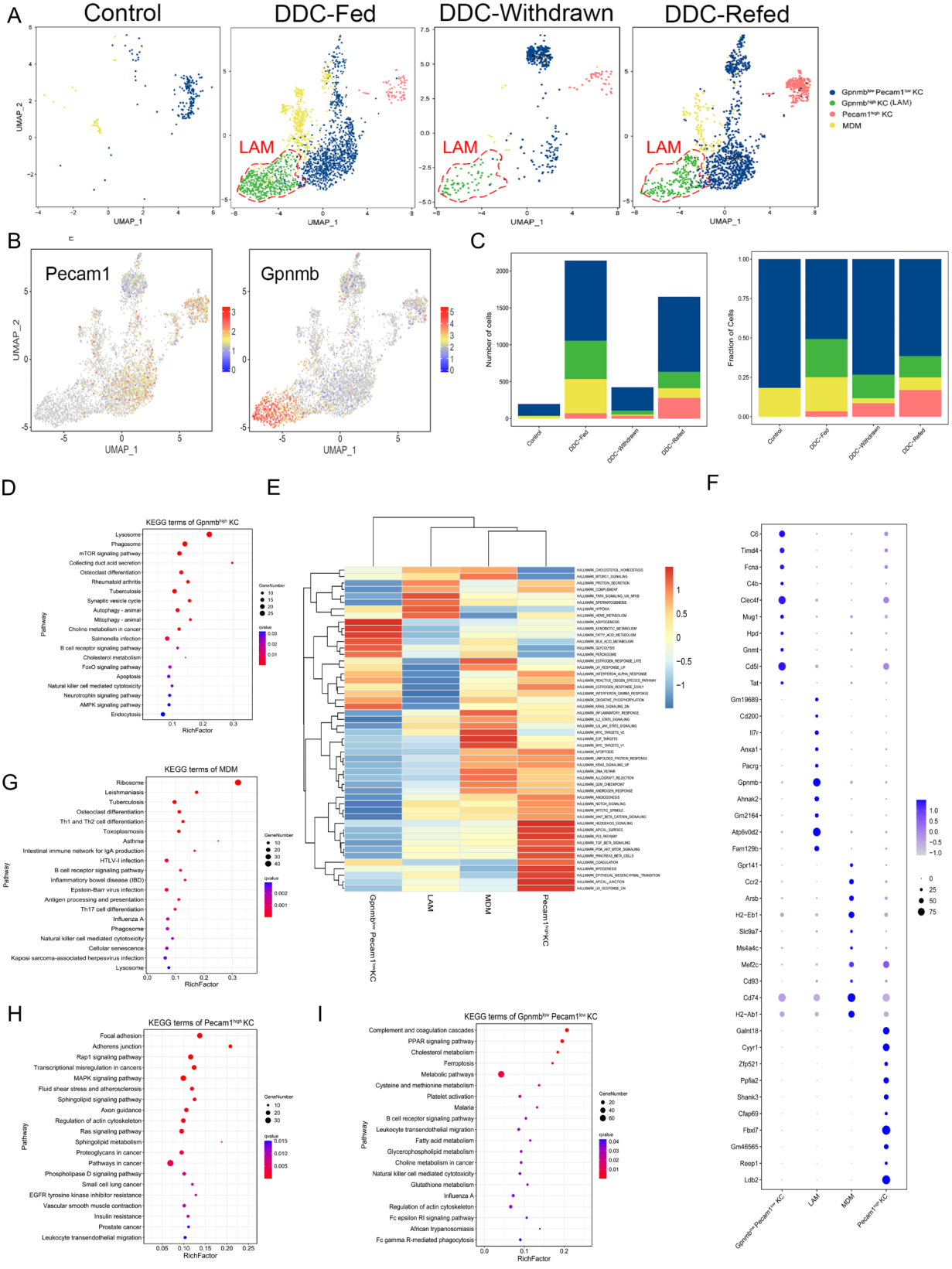


**Fig. 2** (See legend on next page.)

(See figure on previous page.)

**Fig. 2** Clustering and annotation of macrophages transcriptome in DDC mice model. (**A**) UMAP visualization of among Control, DDC-Fed, DDC-Withdrawn, and DDC-Refed mouse livers. (**B**) UMAP plot illustrating feature plots of marker genes. (**C**) Total cell counts and percentage contributions from Control, DDC-Fed, DDC-Withdrawn, and DDC-Refed mouse livers for each subcluster are shown. (**D**) KEGG analysis of the top 20 high expression pathways in Gpnmb$^{high}$ subclusters. (**E**) GSVA showing the differences in pathway activity in four cell subpopulations. The color scale bar indicates increased (red) and decreased (blue) levels. (**F**) Dot-plot showing the top 10 DEGs of MDM, Gpnmb$^{high}$ KC, Pecam1$^{high}$ KC, and Gpnmb$^{low}$ Pecam1$^{low}$ KC macrophage subclusters. Normalized average UMI values for each subcluster were represented by dot size and color intensity. (**G**) KEGG analysis of the top 20 high expression pathways in MDM subclusters. (**H**) KEGG analysis of the top 20 high expression pathways in Pecam1$^{high}$ subclusters. (**I**) KEGG analysis of the top 20 high expression pathways in Gpnmb$^{low}$ Pecam1$^{low}$ KC subclusters

anti-inflammatory phenotype of these macrophages. In addition, the qPCR results showed a dramatic increase in the mRNA expression of Il7r, Cd63, Cd9, Trem2, Gpnmb, Cd200, Pacrg, and Anxa1 in the livers with DDC treatment (Fig. 3C), implying a high relevance between the emergence of LAM and DDC-induced liver injury. We noticed a higher degree expression of Gpnmb in DDC-Withdrawn liver, perhaps because of its complicated paradox in the pro- or anti-inflammatory role [41]. IL-7R is widely expressed in lymphoid lineage and plays a crucial role in immune regulation [38]. We analyzed IL-7R by IHC and noticed that the expression of IL-7R appeared in similar regions of F4/80 positivity (Fig. 3D). Immunofluorescence analysis showed the IL-7R co-localized with GPNMB in macrophages (Fig. 3E). Furthermore, the pie graph showed IL-7R-positive macrophages constitute 59.56% and 26.54% that occurred in the liver of DDC-Fed and DDC-Refed mice of all IL-7R-positive cells (Fig. 3F). To confirm the emergence of IL-7R-positive LAM subset, we observed the enhanced immunoreactivity intensity of IL-7R and GPNMB in HCC patients which had formed MDBs ($n = 3$) (Fig. 3G). These results clearly indicated that the LAM subset in this test featured the expression of IL-7R. A recent study also uncovered a CD127 (an IL-7R subunit) monocyte population, which regulates hypo-inflammatory phenotypes according to STAT5-mediated IL-7 signaling [42]. We next conducted a Kaplan–Meier survival curve of IL-7R, CD200, and ANXA1 analysis in LIHC using GEPIA2 (http://gepia2.cancer-pku.cn/#index) [43]. Interestingly, IL-7R had a protective role in the first eighty months and then a worse survival occurred. Similarly, the results for CD200 and ANXA1 showed higher mortality in the later stages of the disease (Fig. 3G). These results suggested a potential immunosuppressive characterize of these genes and the heterogeneity of LAM, and we considered that LAM might play a protective role during MDBs pathogenesis.

### Macrophages phagocytosed damaged mitochondria in hepatocytes

The formation of MDBs is associated with inflammatory pathways [9]. MDBs were the accumulation of misfolding proteins which might cause a disorder in cells [44], which could improve the cellular stress. Interestingly, mtDNA genes were highly enriched in DDC-induced groups in our database of hepatocytes (Fig. S1A), also GO and KEGG analysis of the distinct subset suggested mitochondrial dysfunction in DDC-treated hepatocytes (Fig. S1B). Then, the transmission electron microscopical analysis was used to explore the ultrastructure in MDB-forming hepatocytes. It showed that in DDC-Fed hepatocytes, the normal mitochondrial cristae structure was disrupted (Fig. 4A). We also observed the swelling endoplasmic reticulum (ER) (Fig. 4B). It implied that the metabolic disorder and release of mtDNA occurred during MDBs pathogenesis. Next, we established an MDB-forming hepa1-6 cell model (Fig. 4C) and qPCR revealed the increased mRNA expression of immunoproteasome genes including Fat10, Mecl-1, Lmp2, and Lmp7 (Fig. 4D). Immunofluorescence staining showed the formation of protein aggresome in the hepa1-6 cells (Fig. 4E). Moreover, the KEGG analysis showed enhanced oxidative phosphorylation in hepatocytes, suggesting the potential presence of oxidized mtDNA (ox-mtDNA) (Fig. S1B). Interestingly, the oxidative stress marker (8-hydroxy-2'-deoxyguanosine, 8-OHdG) was stained for ox-DNA and the damaged DNA was found in the MDB-forming hepa1-6 cells, which localized with p62 and Krt8 (Fig. 4F). To investigate whether macrophages respond to ox-mtDNA released from hepatocytes, we developed a contact co-culture system between Raw 264.7 macrophages and hepa1-6 cells. MitoTracker probes are widely used in live cells to label the mitochondrial membrane. The MDB-forming hepa1-6 labeled by MitoTracker were added to the Raw264.7 for contact co-culture. Immunofluorescence staining showed that MitoTracker Red was detected in F4/80 positive cells, indicating that macrophages phagocytosed the mtDNA released from damaged hepa1-6 (Fig. 4G). These data suggested that MDBs pathogenesis was associated with mtDNA damage, which the damaged hepatocytes could release mtDNA and then activate macrophages.

### NLRP3 inflammasome in macrophage was activated by released mtDNA

During liver injury, mtDNA acts as DAMPs and can activate inflammasomes, such as NLRP3 inflammasomes [45]. GSVA enrichment analysis revealed the activation of hypoxia, inflammatory response, and reactive oxygen species (ROS) pathways (Fig. 2E), which are upstream triggers of inflammasome activation and modulate macrophage functions [46]. UMAP analysis

**Table 4** Total cell counts and percentage contributions from Control, DDC-Fed, DDC-Withdrawn, and DDC-Refed mouse livers for each subcluster

| Cluster | Control | DDC-Fed | DDC-withdrawn | DDC-Refed |
|---|---|---|---|---|
| Total | 197 (100%) | 2140 (100%) | 435 (100%) | 1655 (100%) |
| Gpnmb$^{low}$ Pecam$^{low}$KC | 161 (81.73%) | 1085 (50.7%) | 319 (73.33%) | 1019 (61.57%) |
| LAM Gpnmb$^{high}$KC | 0 (0%) | 519 (24.25%) | 65 (14.94%) | 224 (13.53%) |
| Pecam1$^{high}$KC | 0 (0%) | 72 (3.36%) | 37 (8.51%) | 279 (16.86%) |
| MDM | 36 (18.27%) | 464 (21.68%) | 14 (3.22%) | 133 (8.04%) |

showed the high expression of inflammatory genes in macrophages, indicating a complex interplay between pro- and anti-inflammatory functions (Fig. S2A). Additionally, UMAP analysis further revealed Nlrp3 expression in the Gpnmb$^{low}$ Pecam1$^{low}$ KC and MDM subsets (Fig. S2A). Although we observed high expression of the Aim2 inflammasome (Fig. S2B), our focus remained on the Nlrp3 inflammasome, which is activated by ox-mtDNA. Then, qPCR, Western blot and ELISA verified the activated expression of NLRP3, ASC, pro-IL-1β, and the secretion of IL-1β in protein lysates (Fig. 5A, B, C). While qPCR analysis showed the mRNA expression of caspase-1 was upregulated, the protein levels of pro-caspase-1 did not exhibit a clear trend (Fig. S2C). These results suggested a weak inflammasome activation signal during chronic liver injury. We then used multiplex immunohistochemistry (mIHC) and confirmed that 8-OHdG co-localized with ASC-speck in macrophages (Fig. 5D), indicating that damaged DNA may contribute to inflammasome activation in macrophages during MDBs pathogenesis. Additionally, to investigate macrophage-hepatocyte crosstalk, Raw264.7 macrophages and LPS-primed Raw264.7 macrophages were co-cultured with the Control and MDBs-forming hepa1-6 cells respectively (Fig. 5E). The mRNA expression of Nlrp3, Casp-1, IL-1β in Raw264.7 and LPS primed Raw264.7 was upregulated after co-culturing (Fig. 5F). Additionally, we observed an increase in IL-1β secretion in the supernatant of the LPS-primed co-culture system, whereas IL-1β was absent in the supernatant of the group without LPS priming (Fig. 5G). In the co-culture system without LPS priming, Western blot analysis revealed increased protein levels of NLRP3 and pro-caspase-1 in macrophages (Fig. S3). These findings suggested that MDB-forming hepa1-6 cells may release DAMPs that act as activation signals, inducing the activation of Raw264.7 macrophages. Taken together, these data suggested that damaged mtDNA released from hepatocytes could induce NLRP3 inflammasome activation in liver macrophages, leading to the secretion of IL-1β.

## Discussion

In this study, we performed snRNA-seq to comprehensively understand the heterogeneity of liver macrophage and role of macrophage activation involved in MDBs pathogenesis. Three KC subsets were identified and the changes in these cell types during MDBs formation were investigated. To date, using single-cell transcriptome analyses, Trem2$^+$ Cd63$^+$ Cd9$^+$ Gpnmb$^+$ macrophages have been regarded as classic "Lipid associated macrophages" [47]. Similarly, we found the emergence of a LAM subtype derived from DDC-induced MDBs mouse livers. The LAM subpopulation was defined to respond to local lipid exposure and these macrophages may be a priority for recruitment to the steatotic regions [34]. In addition, the signature genes expressed on LAM are involved in phagocytosis and lipid metabolism whereas the enlarged hepatocytes containing MDBs are often associated with small fat droplet accumulation [48]. These findings suggested that LAM is highly associated with lipid metabolic balance during the MDBs formation process, and they could be recruited to the swollen hepatocytes region and respond to aberrant lipid metabolism. Moreover, tumor-associated macrophages (TAMs) characterized by the expression of Trem2 and Gpnmb, which can develop from monocyte-derived macrophages [33], and these cells share a common signature with LAM. Although we defined LAM derived from resident macrophages, these macrophages with low expression of Timd4 and Ccr2 could receive monocyte contribution and were not continuously refreshed [49]. The M2-like phenotype macrophages have a dominant role in the progression of HCC [42]. Consistent with this, LAM cells expressed many genes linked with anti-inflammation (e.g. IL-7R, Cd200, and Anxa1) in our snRNA-seq database, suggesting they may be involved in modulating inflammatory response during MDBs formation. The Kaplan–Meier survival analysis suggested a potential immunosuppressive character of LAM in our data. However, whether LAM is influenced by lipids to deliver anti-inflammatory signals and protect the liver during MDBs pathogenesis needs to be determined.

Our previous C57BL/6 mice of snRNA-seq profile revealed a Ccr2$^+$ inflammatory phenotype macrophage [28]. Similarly, our study also illustrated MDM which might be recruited by tissue damage and increased pro-inflammatory response to drive the progression of MDBs formation. CCR2 and its ligand CCL2 (chemokine ligand 2) are implicated to be a key factor of monocyte infiltration, and it has been found in preclinical animal models

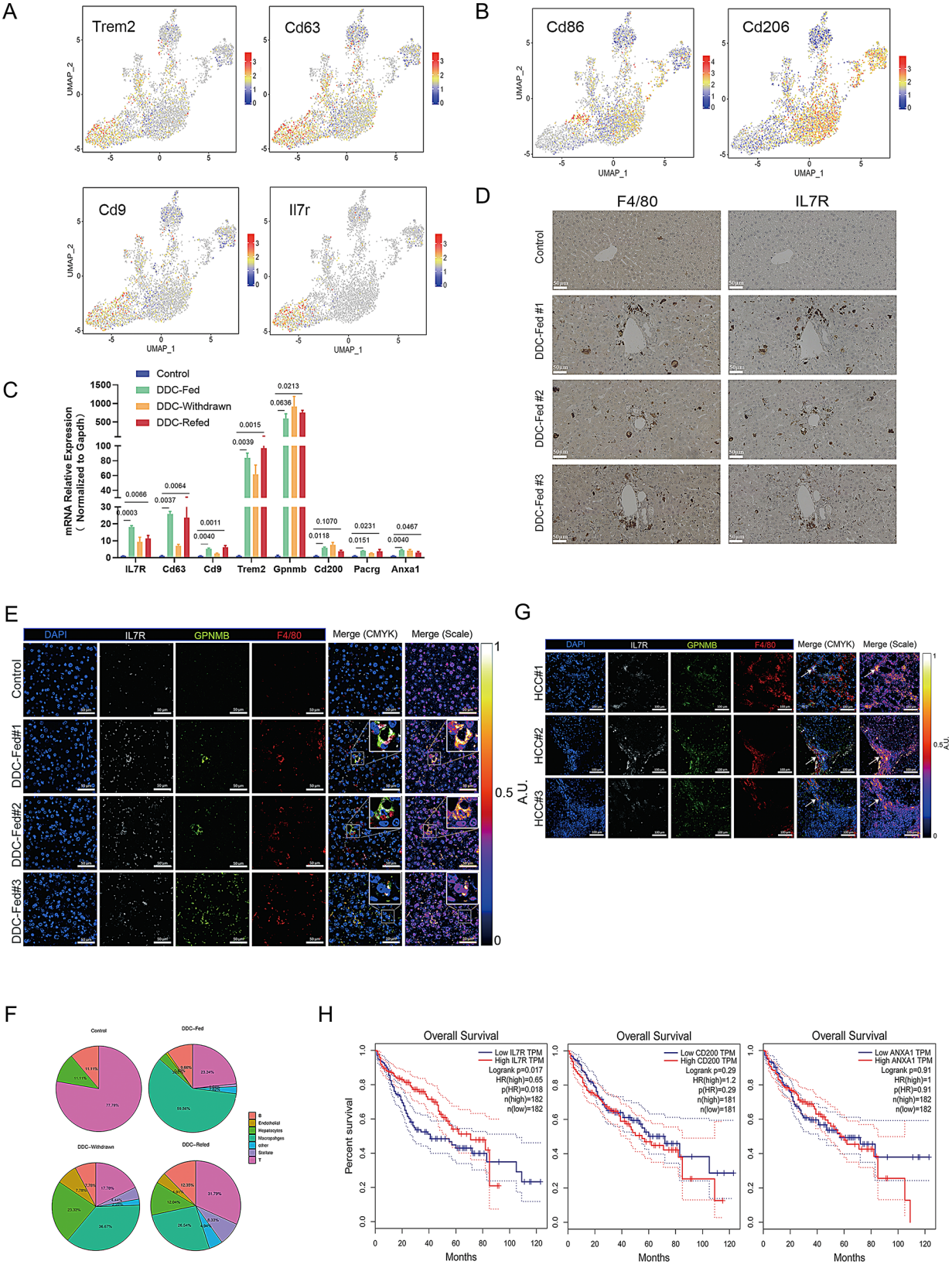


**Fig. 3** (See legend on next page.)

(See figure on previous page.)

**Fig. 3** Featured marker genes and abnormally expressed genes in LAM. (**A**) UMAP plot illustrating feature plots of marker genes Trem2, Cd63, Cd9, and IL-7R expression. (**B**) UMAP plot showing feature plots M1 phenotype genes and M2 phenotype genes. low (grey) and high (red). (**C**) LAM surface marker genes of Control, DDC-Fed, DDC-Withdrawn, and DDC-Refed mice liver tissue were detected by qPCR. The DDC-Fed and DDC-Refed groups were compared to the Control group. Data are shown as mean ± SEM, and P-values were determined by one-way ANOVA of independent biological experiments ($n = 3$). (**D**) Immunohistochemical analysis of F4/80 and IL-7R expression in Control and DDC-Fed liver tissue sections are shown. Scale bar = 50 μm. (**E**) Confocal immunofluorescence images of tissue sections from Control and DDC-fed groups with DAPI (blue, 405 nm), IL-7R (white, 633 nm), GPNMB (green, 488 nm), and F4/80 (red, 561 nm). Images were taken with a 40×/0.95 NA objective lens. Scale bar = 50 μm. (**F**) The Pie graph shows the percentages of each cell type in total IL-7R-positive cells from Control, DDC-Fed, DDC-Withdrawn, and DDC-Refed mouse livers. (**G**) Confocal immunofluorescence images for DAPI (blue, 405 nm), IL-7R (white, 633 nm), GPNMB (green, 488 nm), and F4/80 (red, 561 nm) in liver sections from HCC patients. Images were taken with a 20×/0.8 NA objective lens. Scale bar = 100 μm. (**H**) Kaplan–Meier survival curve of IL-7R, CD200, and ANXA1 expression using the optimal group cut-off point in patients with LIHC (the original database was downloaded from TCGA, and the curves were obtained using GEPIA). p values were obtained from 2-sided log-rank tests

that blockade of CCL2-CCR2-mediated macrophage infiltration could alleviate the NASH and fibrosis [50]. A recent report used Ccr2 KO mice to unravel that the LAM may be derived from monocytes and the process may be enhanced by tissue damage and lipid accumulation [51]. This observation indicated the relevance of MDM with MDBs pathogenesis. In contrast, the IL7R-positive LAM subset was not identified in our previous research. In the previous study, we identified a potential subset that aligns with the findings of current study (Figure S4). We also recognized another two functionally distinct KC subsets including $Pecam^{high}$ KC and $Gpnmb^{low}$ $Pecam1^{low}$ KC that might play a regulatory role in the immune response and infiltration. Collectively, our data characterized the heterogeneity of macrophages and could help to study the immune microenvironment during the formation of MDBs.

Cellular stress and senescence are the characteristics of MDBs [2]. Here, we observed the damaged ER and mitochondria by electron microscopy in the MDBs mice model, indicating ER stress and mitochondrial dysfunction. The ER carries out the functions of protein folding and assembly, calcium storage, and lipid synthesis [52, 53]. Interestingly, both MDM and $Pecam1^{high}$ KC shared common signatures in GSVA such as unfolded protein response (UPR) and DNA repair pathway, suggesting the subsets might be involved in MDBs formation. UPR acts as a guardian of the ER to activate the accumulation of misfolded proteins while the MDBs were the misfolded protein aggresomes, suggesting a specific activation at the molecule level. Therefore, UPR and DNA repair pathways enriched in GSVA also gave us a new insight into considering the close relationship between MDBs formation and ER stress.

Mitochondrial dysfunction implies the depletion and release of mtDNA and would lead to damage to membrane proteins and lipids. Recently, researchers have shown that mtDNA released from injured cells can act as DAMPs to trigger inflammasomes in liver non-parenchymal cells (NPCs), which may promote inflammation and exacerbate hepatocellular damage [45]. An earlier study has confirmed the increased expression of IL-1β in DDC-feeding mice [54]. In this study, we confirmed the activation of ASC-containing inflammasome complexes that indicate the activation of inflammasome and the release of IL-1β. IL-1β can continuously bind to its receptor IL-1R1, leading to the activation of classic NF-κB inflammatory signaling [55]. Furthermore, the MDBs could result in the IκBα-sequestration leading to protein aggregate-induced inflammation [10]. While activation of NF-κB is essential for MDB formation [9]. This implies a possible activated pathway leading to increased liver injury and shows a high correlation between inflammasome activation and MDBs progression. During the progression of chronic liver injury, macrophages dynamically participate in chronic inflammation and might act as a bridge for hepatocyte injury signaling. However, the origin of damaged mtDNA that activates the macrophages in the livers of mice needs to be determined. Additionally, the increase of NF-κB in DDC-Fed mice has been confirmed to promote inflammatory factors such as TNFα and IFNγ, which could help the growth of FAT10-positive cells. The FAT10-positive hepatocytes were more likely to form MDBs, and the IFNγ played a crucial role in the switch of the catalytic subunits from the 26s proteasome and promoted the MDBs formation [9]. Based on the current information, upon chronic liver injury, the mtDNA in hepatocytes are released from the damaged mitochondrion into extracellular. Then, the DNA sensor NLRP3 on macrophages was activated to form ASC-speck and the subsequent catalytically activation of caspase-1 for IL-1β, leading to MDBs formation (Fig. 5H).

However, we are aware of some limitations in the current study. The DDC-induced mouse MDBs model of chronic liver injury only exhibits part of the clinical pathological phenotypes. Further investigations need to explore the more pathological phenotypes to explain the MDBs pathogenesis using various diets combined with DDC. Additionally, the mechanism of IL-1β secretion need to be further determined between hepatocytes and nonparenchymal cells, such as hepatic stellate cells, since hepatic stellate cells activation will provide additional paracrine signals (cytokines, chemokines, etc.) to promote MDBs formation. Finally, our findings have

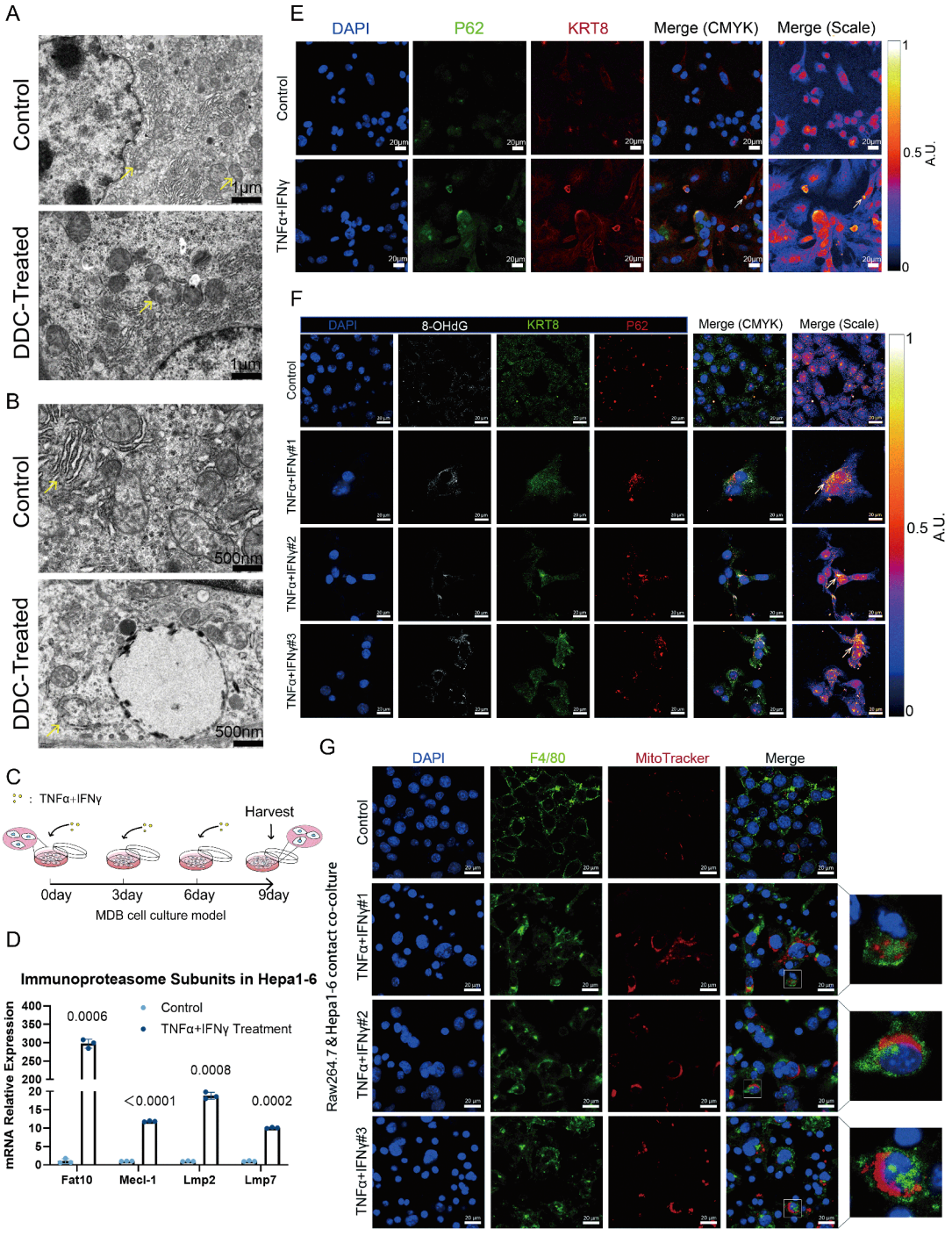


**Fig. 4** The released mtDNA phagocytosed by Raw264.7 cells. (**A**) Transmission electron micrographs of hepatocytes in mouse liver, and yellow arrows indicate the normal and damaged mitochondria. Mag: 5000× (**B**) Transmission electron micrographs of hepatocytes in mouse liver, and yellow arrows indicate the normal and swelling endoplasmic reticulum.Mag: 5000× (**C**) Schematic construction of MDB-forming hepa1-6 cells cell model. (**D**) The mRNA expressions of Fat10, Lmp2, Lmp7, and Mecl-1 in Hepa1-6 cells were analyzed by qPCR. Data are shown as mean ± SEM, and P-values were determined by unpaired two-tailed Student's t-test of independent biological experiments ($n = 3$). (**E**) Confocal immunofluorescence staining for DAPI (blue, 405 nm), p62 (green, 488 nm), and Krt8 (red, 561 nm) co-localized with aggresomes (white arrows) in the Control group and TNFα + IFNγ group were shown. Images were taken with a 63×/1.4 NA oil objective lens. Scale bar = 20 μm. (**F**) Confocal immunofluorescence staining for co-localization of DAPI (blue, 405 nm), 8-OHdG (white, 633 nm), p62 (red, 561 nm), and Krt8 (green, 488 nm) of the Control group and TNFα + IFNγ group were shown. Images were taken with a 63×/1.4 NA oil objective lens. Scale bar = 20 μm. (**G**) Confocal immunofluorescence staining of contact co-culture, DAPI (blue, 405 nm), F4/80 (green, 488 nm), and MitoTracker (red, 561 nm). The macrophages phagocytose the mtDNA released from damaged hepa1-6. Images were taken with a 63×/1.4 NA oil objective lens. Scale bar = 20 μm

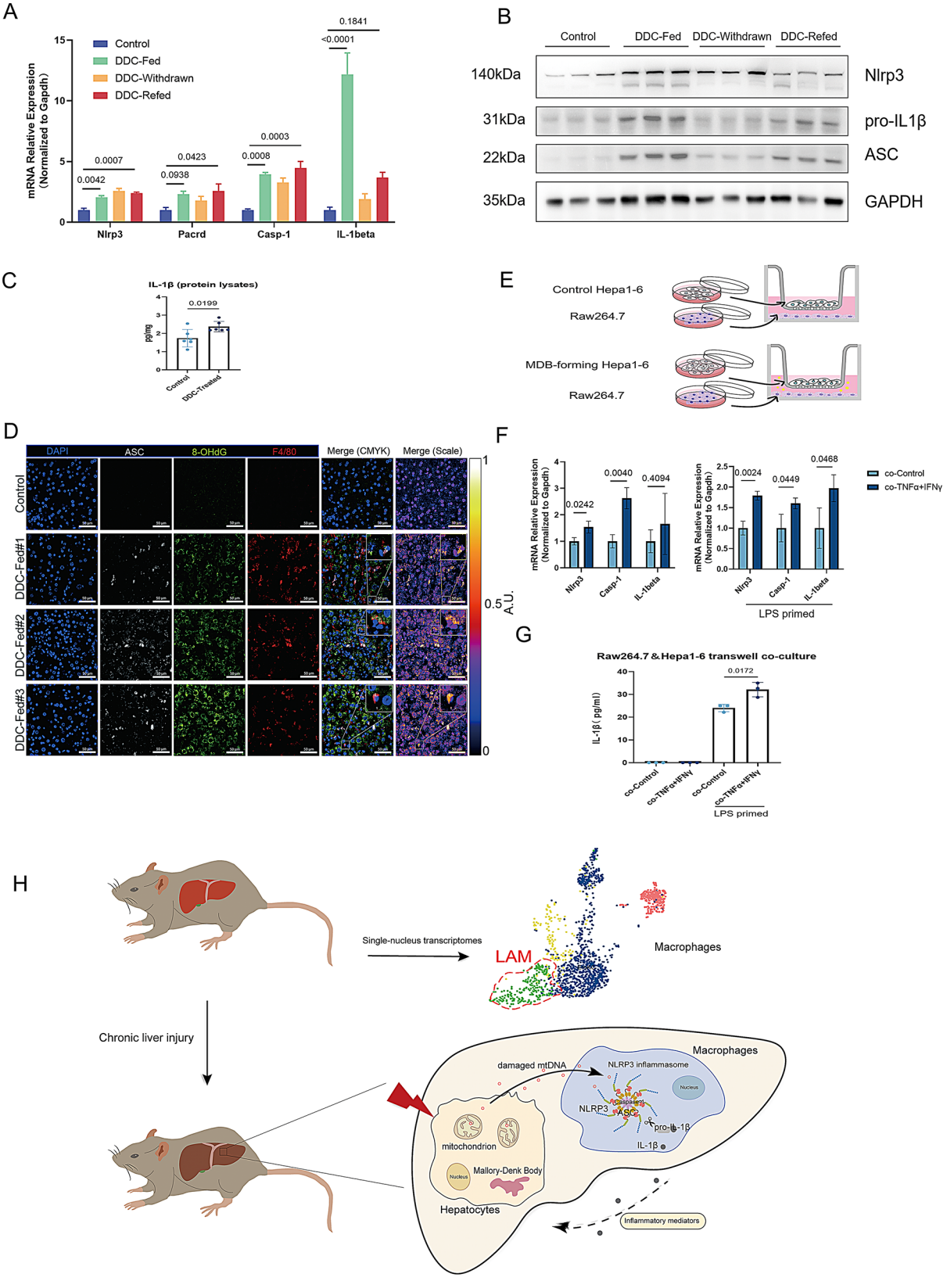


**Fig. 5** (See legend on next page.)

(See figure on previous page.)

**Fig. 5** Damaged DNA actived NLRP3 inflammasome in macrophages. (**A**) The genes of inflammasomes were detected in Control, DDC-Fed, DDC-Withdrawn, and DDC-Refed mice liver tissue by qPCR. The DDC-Fed and DDC-Refed groups were compared to the Control group. Data are shown as mean ± SEM, and P-values were determined by one-way ANOVA of independent biological experiments ($n = 3$). (**B**) Immunoblot analysis of total lysates from liver tissue of Control, DDC-Fed, DDC-Withdrawn, and DDC-Refed mice. (**C**) IL-1β secretion from the protein lysates of Control and DDC-treated mice was determined by ELISA. (**D**) Confocal immunofluorescence staining for DAPI (blue, 405 nm), ASC (white, 633 nm), 8-OHdG (green, 488 nm), and F4/80 (red, 561 nm) in sections from Control and DDC-Fed tissue are shown. Images were taken with a 40×/0.95 NA objective lens. Scale bar = 50 µm. (**E**) An illustration of the transwell co-culture system, the Control hepa1-6 or MDB-forming hepa1-6 were added in the up chamber and then co-cultured with Raw264.7 cells seeding in the low chamber. (**F**) qPCR analysis of the mRNA expression of Nlrp3, Casp-1, and IL-1β in Raw264.7 cells. Data are shown as mean ± SEM, and P-values were determined by unpaired two-tailed Student's t-test of independent biological experiments ($n = 3$). (**G**) The secretion of IL-1β in the supernatants of the co-culture system was detected by ELISA. Data are shown as mean ± SEM, and P-values were determined by unpaired two-tailed Student's t-test of independent biological experiments ($n = 3$). (**H**) A proposed working model illustrates that the mtDNA in MDB-forming hepatocytes was released from the damaged mitochondrion into the cytosol. Subsequently, the NLRP3 on macrophages were activated to form ASC-speck leading to the secretion of IL-1β and contribute to MDBs formation

not been sufficiently validated in all human chronic liver disease. Further evidence from other human samples is needed.

In summary, this study reveals for the first time hepatic macrophage heterogeneity in MDBs pathogenesis and helps to better understand the mechanism of chronic liver disease. Specifically, a classic LAM was revealed to be involved in MDBs formation, characterized by high IL-7R expression in our transcriptome data, showing a potential anti-inflammatory characteristic. Additionally, the Gpnmb$^{low}$ Pecam1$^{low}$ KC, Pecam1$^{high}$ KC, and MDM subsets were found to be expanded, promoting inflammation. These findings implied that macrophages exhibit dual roles—pro-inflammatory and anti-inflammatory—that dynamically shift in response to distinct injury signals at various stages of disease progression. Furthermore, the MDB-forming hepatocytes were associated with cellular stress and the hepatocytes release mtDNA to trigger the activation of inflammasome in macrophages, providing better understanding for molecular mechanism of chronic liver disease.

### Financial support

The research was supported by the National Key Research and Development Program of China (No. 2022YFC2304800). This work was supported by the research funding the Grant No. 2021KSYS009 from Key Laboratory of Guangdong Higher Education Institutes, by the foundation of Guangzhou Key Laboratory of Biological Targeting Diagnosis and Therapy (No. 202201020379), Key-Area Research and Development Program of Guangdong Province (No. 2022B1111020002), and supported by the open research funds under Grant Number 202301-205 from the Affiliated Qingyuan Hospital of Guangzhou Medical University, Qingyuan People's Hospital. The research was also supported by the funds under Grant Number 2024SRP133 from the fifth Affiliated Hospital of Guangzhou Medical University. We are grateful to thank Guangzhou Genedenovo Biotechnology Co., Ltd for assisting in sequencing and bioinformatics analysis. We thank Editage (www.editage.cn) for English language editing.

**Abbreviations**

| | |
|---|---|
| ASC | Apoptosis-associated speck-like protein containing a caspase recruit domain |
| ASH | Alcoholic steatohepatitis |
| DDC | Diethyl 1, 4-dehydro-2, 4, 6-trimethyl-3, 5-pyridine-dicarboxylate |
| GSVA | Gene set variation analysis |
| HCC | Hepatocellular carcinoma |
| IL-1β | Interleukin-1beta |
| IL-7R | Interleukin-7 recepter |
| KEGG | Kyoto Encyclopedia of Genes and Genomes |
| MDBs | Mallory-Denk bodies |
| mtDNA | Mitochondrial DNA |
| NASH | Non-alcoholic-associated steatohepatitis |
| NLRP3 | NOD-like receptor family pyrin domain containing-3 |
| qPCR | Quantitative real-time polymerase chain reaction |
| snRNA-seq | Single-nucleus RNA sequencing |

## Supplementary Information

The online version contains supplementary material available at https://doi.org/10.1186/s12967-024-05999-7.

Supplementary Material 1: Figure S1: Potential Link Between MDBs Formation and Mitochondrial Dysfunction. A: Dot-plot showing the top 10 DEGs of hepatocyte subset. Normalized average UMI values for each subcluster were represented by dot size and color intensity. B: GO and KEGG analysis of the top 20 high expression pathways in the Hep5 cluster.

Supplementary Material 2: Figure S2: Differential Expression of Inflammatory Genes in Macrophages. A: UMAP plot illustrating feature plots of inflammatory genes Nlrp3, Aim2, Nfkb1, Tgfb1, Tnfaip2 and Tnfaip8 expression. B: The Aim2, and other inflammasome genes were detected in Control, DDC-Fed, DDC-Withdrawn, and DDC-Refed mice liver tissue by qPCR. The DDC-Fed and DDC-Refed groups were compared to the Control group. Data are shown as mean ± SEM, and P-values were determined by one-way ANOVA of independent biological experiments (n=3). C: Immunoblot analysis of pro-Caspase-1 and cleaved-caspase-1 in total lysates from liver tissue of Control, DDC-Fed, DDC-Withdrawn, and DDC-Refed mice.

Supplementary Material 3: Figure S3: Activation of the Inflammasome in Co-Culture System. Immunoblot analysis of NLRP3 and pro-caspase-1 in total lysates of macrophages from a co-culture system without LPS priming. Quantification of Western blot band intensities for NLRP3 and pro-caspase-1 is shown in the bar graph. Protein levels were normalized to β-actin and expressed as fold changes relative to the control group. Data are shown as mean ± SEM, and P-values were determined by unpaired two-tailed Student's t-test of independent biological experiments (n=3)

Supplementary Material 4: Figure S4: UMAP plot illustrating feature plots of marker genes Trem2, Cd63, Cd9, and Il-7r expression, based on publicly available RNA-seq data (GSE228448).

Supplementary Material 5

Supplementary Material 6

Supplementary Material 7

Supplementary Material 8

Supplementary Material 9

**Authors' contributions**
L.H. and T.X.P. designed and supervised the experiments, and analyzed and interpreted the data. L.H. and F.Z.X. wrote the manuscript. F.Z.X., S.Y., Z.W.M. performed the cellular and most mouse experiments and prepared figures. F.Z.X., and Z.B., analyzed the single-cell sequencing data. S.Y., and Z.W.M did the western blot analysis. H.M.P. did immunostaining analysis. F.Z.X. did data analysis and all authors reviewed the manuscript.

## Declarations

**Conflict of interest**
The authors of this manuscript have no conflict of interest to disclose.

Received: 3 July 2024 / Accepted: 15 December 2024
Published online: 16 January 2025

**References**

1. Zatloukal K, et al. From Mallory to Mallory–Denk bodies: what, how and why? Exp Cell Res. 2007;313(10):2033–49.
2. Denk H, Abuja PM, Zatloukal K. Mallory-Denk bodies and hepatocellular senescence: a causal relationship? Virchows Archiv; 2024.
3. Basaranoglu M, et al. Mallory-Denk bodies in chronic hepatitis. World J Gastroenterol. 2011;17(17):2172–7.
4. French SW, Mendoza AS, Peng Y. The mechanisms of Mallory-Denk body formation are similar to the formation of aggresomes in Alzheimer's disease and other neurodegenerative disorders. Exp Mol Pathol. 2016;100(3):426–33.
5. Hanada S, et al. The genetic background modulates susceptibility to mouse liver Mallory-Denk body formation and liver injury. Hepatology. 2008;48(3):943–52.
6. Vogel A, et al. Hepatocellular carcinoma. Lancet. 2022;400(10360):1345–62.
7. Li J, et al. S-adenosylmethionine prevents mallory denk body formation in drug-primed mice by inhibiting the epigenetic memory. Hepatology. 2007;47(2):613–24.
8. Kucukoglu O, et al. High-fat diet triggers Mallory-Denk body formation through misfolding and crosslinking of excess keratin 8. Hepatology. 2014;60(1):169–78.
9. French SW. Mallory-Denk body pathogenesis revisited. World J Hepatol, 2010. 2(8).
10. Liu Y, et al. A novel mechanism for NF-κB-activation via IκB-aggregation: implications for hepatic Mallory-Denk-Body Induced inflammation. Mol Cell Proteom. 2020;19(12):1968–86.
11. de Carvalho Ribeiro M, Szabo G. Role of the Inflammasome in Liver Disease. Annu Rev Pathol. 2022;17:345–65.
12. Yadav P, et al. Therapeutic potential of stem cells in regeneration of liver in chronic liver diseases: current perspectives and future challenges. Pharmacol Ther. 2024;253:108563.
13. Kandel-Kfir M, et al. IFNγ potentiates TNFα/TNFR1 signaling to induce FAT10 expression in macrophages. Mol Immunol. 2020;117:101–9.
14. Oliva J, et al. The role of cytokines in UbD promoter regulation and Mallory-Denk body-like aggresomes. Exp Mol Pathol. 2010;89(1):1–8.
15. Lee J, et al. The liver is populated by a broad spectrum of markers for macrophages. In alcoholic hepatitis the macrophages are M1 and M2. Exp Mol Pathol. 2014;96(1):118–25.
16. Fukushima H, et al. Formation of p62-positive inclusion body is associated with macrophage polarization in non-alcoholic fatty liver disease. Hepatol Res. 2018;48(9):757–67.
17. Dou L et al. Macrophage phenotype and function in liver disorder. Front Immunol, 2020. 10.
18. Matsuda M, Seki E. Hepatic stellate cell–macrophage crosstalk in liver fibrosis and carcinogenesis. Semin Liver Dis. 2020;40(03):307–20.
19. Kourtzelis I, Hewitson J, Roger T. Editorial: macrophage plasticity in sterile and Pathogen-Induced inflammation. Front Immunol, 2021. 12.
20. de Cavanagh EMV, et al. Renin–angiotensin system inhibitors protect against age-related changes in rat liver mitochondrial DNA content and gene expression. Exp Gerontol. 2008;43(10):919–28.
21. Fang C, Wei X, Wei Y. Mitochondrial DNA in the regulation of innate immune responses. Protein Cell. 2016;7(1):11–6.
22. Hu Q et al. The role of mitochondrial DNA in the development of Ischemia Reperfusion Injury. Shock, 2019. 51(1).
23. Oka T, et al. Mitochondrial DNA that escapes from autophagy causes inflammation and heart failure. Nature. 2012;485(7397):251–5.
24. Peng Y, et al. The inflammasome in alcoholic hepatitis: its relationship with Mallory–Denk body formation. Exp Mol Pathol. 2014;97(2):305–13.
25. Andrews TS, et al. Single-Cell, Single-Nucleus, and spatial RNA sequencing of the Human Liver identifies cholangiocyte and mesenchymal heterogeneity. Hepatol Commun. 2021;6(4):821–40.
26. Yang L, et al. Determination of key events in mouse hepatocyte maturation at the single-cell level. Dev Cell. 2023;58(19):1996–2010.e6.
27. Alvarez M, et al. Human liver single nucleus and single cell RNA sequencing identify a hepatocellular carcinoma-associated cell-type affecting survival. Genome Med. 2022;14(1):50.
28. Zhang R, et al. Single-cell transcriptomes identifies characteristic features of mouse macrophages in liver Mallory-Denk bodies formation. Experimental and Molecular Pathology; 2022. p. 127.
29. Guillot A, Tacke F. Liver macrophages: Old dogmas and New insights. Hepatol Commun. 2019;3(6):730–43.
30. Wen Y, et al. Hepatic macrophages in liver homeostasis and diseases-diversity, plasticity and therapeutic opportunities. Cell Mol Immunol. 2020;18(1):45–56.
31. Hosseini N, Shor J, Szabo G. Alcoholic Hepatitis: Rev Alcohol Alcohol. 2019;54(4):408–16.
32. Huby T, Gautier EL. Immune cell-mediated features of non-alcoholic steatohepatitis. Nat Rev Immunol. 2022;22(7):429–43.
33. Yan J, Horng T. Lipid metabolism in regulation of macrophage functions. Trends Cell Biol. 2020;30(12):979–89.
34. Guilliams M, et al. Spatial proteogenomics reveals distinct and evolutionarily conserved hepatic macrophage niches. Cell. 2022;185(2):379–e39638.
35. Watt SM, Gschmeissner SE, Bates PA. PECAM-1: its expression and function as a cell adhesion molecule on hemopoietic and endothelial cells. Leuk Lymphoma. 1995;17(3–4):229–44.
36. Jaitin DA, et al. Lipid-Associated Macrophages Control Metabolic Homeostasis in a Trem2-Dependent manner. Cell. 2019;178(3):686–e69814.
37. Horn CL et al. Role of cholesterol-Associated Steatohepatitis in the development of NASH. Hepatol Commun, 2022. 6(1).
38. Wang C et al. The role of IL-7 and IL-7R in Cancer Pathophysiology and Immunotherapy. Int J Mol Sci, 2022. 23(18).
39. Kotwica-Mojzych K, Jodłowska-Jędrych B, Mojzych M. *CD200:CD200R Interactions and Their Importance in Immunoregulation.* Int J Mol Sci, 2021. 22(4).
40. Li L, et al. The role of ANXA1 in the tumor microenvironment. Int Immunopharmacol. 2024;131:111854.
41. Saade M, et al. The role of GPNMB in inflammation. Front Immunol. 2021;12:674739.
42. Zhang B et al. CD127 imprints functional heterogeneity to diversify monocyte responses in inflammatory diseases. J Exp Med, 2022. 219(2).
43. Tang Z, et al. GEPIA: a web server for cancer and normal gene expression profiling and interactive analyses. Nucleic Acids Res. 2017;45(W1):W98–102.
44. Strnad P, et al. Intermediate filament cytoskeleton of the liver in health and disease. Histochem Cell Biol. 2008;129(6):735–49.
45. Zhang X et al. Mitochondrial DNA in liver inflammation and oxidative stress. Life Sci, 2019. 236.
46. Jung E, et al. Chronic hypoxia of endothelial cells boosts HIF-1α-NLRP1 circuit in Alzheimer's disease. Free Radic Biol Med. 2023;204:385–93.
47. Vonderlin J, et al. The multifaceted roles of macrophages in NAFLD Pathogenesis. Cell Mol Gastroenterol Hepatol. 2023;15(6):1311–24.
48. Caldwell S, et al. Hepatocellular ballooning in NASH. J Hepatol. 2010;53(4):719–23.
49. Dick SA, et al. Three tissue resident macrophage subsets coexist across organs with conserved origins and life cycles. Sci Immunol. 2022;7(67):eabf7777.
50. Lefere S, Devisscher L, Tacke F. Targeting CCR2/5 in the treatment of nonalcoholic steatohepatitis (NASH) and fibrosis: opportunities and challenges. Expert Opin Investig Drugs. 2020;29(2):89–92.
51. Daemen S, et al. Dynamic shifts in the composition of Resident and Recruited Macrophages Influence Tissue Remodeling in NASH. Cell Rep. 2021;34(2):108626.

52. Di Conza G, Ho P-C. ER stress responses: an emerging modulator for innate immunity. Cells, 2020. 9(3).
53. Hetz C, Zhang K, Kaufman RJ. Mechanisms, regulation and functions of the unfolded protein response. Nat Rev Mol Cell Biol. 2020;21(8):421–38.
54. Bardag-Gorce F, et al. SAMe prevents the up regulation of toll-like receptor signaling in Mallory-Denk body forming hepatocytes. Exp Mol Pathol. 2010;88(3):376–9.
55. Pan J, et al. Transmission of NLRP3-IL-1β signals in Cerebral Ischemia and Reperfusion Injury: from Microglia to adjacent neuron and endothelial cells via IL-1β/IL-1R1/TRAF6. Mol Neurobiol. 2023;60(5):2749–66.

## Publisher's note